Behrens, U.; Díaz Calleja, R.; Dötze, M.; Franke, U.; Gunsser, W.; Klar, G.; Kudnig, J.... (1996). Structure, dielectric relaxation and electrical conductivity of 2,3,7,8-Tetramethoxychalcogenanthrene-2,3-dichloro-5,6-dicyano-1,4-benzoquinone 1:1 charger-transfer complexes. Journal of Materials Chemistry. 6(4):547-553. https://doi.org/10.1039/JM9960600547

Structure, Dielectric Relaxation and Electrical Conductivity of the 2,3,7,8-Tetramethoxychalcogenanthrene–2,3-Dichloro-5,6-dicyano-1,4-benzo-quinone 1:1 Charge-transfer Complexes

Ulrich Behrens[a], Ricardo Díaz Calleja*[c], Mark Dötze[c], Ursula Franke[b], Walter Gunβer[b], Günter Klar*[a], Jens Kudnig[a], Falk Olbrich[a], Enrique Sánchez Martínez[d], Maria J. Sanchis[c], Bärbel Zimmer[a]

[a]*Institut für Anorganische und Angewandte Chemie der Universität Hamburg, Martin-Luther-King-Platz 6,* [b]*Institut für Physikalische Chemie der Universität Hamburg, Bundesstraβe 45, D-20146 Hamburg, Germany.*

[c]*Departamento de Termodinámica Aplicada. E.T.S.I.I. and* [d]*Departamento de Ingeniería Electrónica. E.T.S.I.T. ,Universidad Politécnica de Valencia, Camino de Vera, s/n, E-46071 Valencia, Spain.*

2, 3, 7, 8-Tetramethoxychalcogenanthrenes (5,10-chalcogena-*cyclo*-diveratrylenes, "Vn_2E_2", E = S, Se) form isotypical 1:1 charge-transfer (CT) complexes with 2,3-dichloro-5,6-dicyano-1,4-benzoquinone (DDQ). X-Ray analysis of Vn_2S_2·DDQ shows the compound to have a columnar structure with segregated stacks of donors and acceptors. The donors are virtually planar in accordance with a formulation as $[Vn_2E_2]^+$ $[DDQ]^-$. Both, donor cations and acceptor anions are equidistantly arranged in their respectively stacks, but in each case inclined to the staking axis, nevertheless guaranteeing an optimum overlap of the half-filled frontier orbitals which are of π-type character according to MNDO calculations.

Dielectrical ac measurements of permittivity ε' and loss factor ε'' clearly reveal two processes, a dielectric one at low and a conductive one at high temperatures. The dielectric process can be described by the Havriliak-Negami (HN) and the Kohlrausch-Williams-Watts (KWW) model as well, the conductive process by a Debye-type plot. By this, the revelant parameters are evaluated.

The dc conductivities of polycrystalline samples moulded at 10^8 Pa show a temperature dependence in the ln σ vs T^{-1} diagrams which is typical for semiconductors. Two slopes are found; that in the low temperature region (<285K) is explained by a easy-path model (intragrain conductivity with low activation energies), whereas in the high-temperature region conduction accross the grain boundaries (with higher activation energies) is becoming predominant. The activation energies for the intrinsic conductivities obtained by the ac and dc measuremets are close to each other. Despite the columnar structure with segregated stacks, due to stoichiometric oxidation states of the components, the absolute values of the conductivity are low (*ca.* 10^{-6} S cm^{-1} at 293K), though by a factor of *ca.* 10^3 higher than those of compounds like Vn_2E_2·TCNQ with stacks in which donor and acceptor molecules alternate.

The electron-rich 2,3,7,8-tetramethoxychalcogenanthrenes (5,10-dichalcogena-*cyclo*-divera-trylenes, "Vn_2E_2", E = S, Se) act as donors in charge-transfer (CT) complexes. With tetracyanoethene (TCNE) the complexes $2Vn_2E_2 \cdot$TCNE are formed which in their solid states possess stacks of Vn_2E_2 | TCNE | Vn_2E_2 units.[2] With 7,7,8,8-tetracyanoquinodimethane (TCNQ) 1:1 complexes are obtained in the stacks of which donor and acceptor molecules alternate.[3] As a consequence of their crystal structures both types of compounds show only poor electrical conductivity.[2, 4, 5]

[Formulae Vn_2E_2, TCNE, TCNQ, DDQ]

Using 2,3-dicyano-5,6-dichloro-1,4-benzoquinone (DDQ) as a further acceptor, 1:1 complexes were formed with Vn_2E_2 which are isotypical for E=S and E=Se.[6] The dark blue compounds were easily prepared by combining the hot solutions in acetonitrile. In the case of the sulfur compound also single crystals suitable for a crystal structure determination could be obtained.

Crystal Structure Determination of $Vn_2S_2 \cdot$DDQ

A Siemens P4 four circle diffractometer (MoKα radiation with λ= 71.073 pm, $\omega/2\theta$ scan mode, Lorentz and polarization corrections) and the program Siemens SHELXTL-Plus (VMS)[7] were used for the X-ray analysis. The structure was determinated by direct methods. Fourier syntheses allowed the positions of all non-hydrogen atoms to be determined; these atom positions were refined with anisotropic temperature factors. The positions of the hydrogen atoms were calculated with fixed distances of 105 pm and isotropic temperature factors. The results are given in Tables 1 and 2.*

* Supplementary data avilable from the Cambridge Crystallographic Data Centre: see Information for Authors, *J. Mater. Chem.*, 1995, Issue 1.

Description of the Structure

Molecular Structure

The asymmetric unit of Vn_2S_2·DDQ contains half a molecule of each component, the molecular structures of which are shown in Fig. 1.

[Fig.1]

The outstanding feature of the donor is its planarity, although the thermal parameters of the sulfur atoms indicate that they may be disordered with deviations of maximum ±20 pm from the best planes of the two aryl rings. By this a formulation of the complex according to $[Vn_2S_2]^+[DDQ]^-$ is suggested. Namely, whereas the neutral Vn_2S_2 molecule is folded at the SS axis (angle of fold, defined as the angle between the normals to the best planes of the aryl rings: φ = 131° and 128° for the monoclinic[8] and orthorhombic[9] forms, respectively), its monocation $[Vn_2S_2]^+$ is planar (φ = 180°)[10] and any partially oxidized form $[Vn_2S_2]^{x+}$ ($0<x<1$) as in $2Vn_2S_2$·TCNE or Vn_2S_2·TCNQ has angles between these values.[2,3] These observations correlate well with the oxidation potentials E_1 of these acceptors (+0.51 V for DDQ , +0.15 V for TCNE and +0.17V for TCNQ , each *vs.* sce). [11, 12]

In the levelling of the donor molecule the methoxy substituents are included, *i.e.* each pair of ortho-standing methoxy groups is coplanar with its aryl ring, both in *exo*-positions, thus facilitating the formation of stacks in the crystal. For other derivatives of Vn_2S_2 this behaviour has also been found[2,3] ; the consequences with respect to bond lengths and angles have already been discussed in connection with the structure of Vn_2S_2 itself [8] (Table 3).

[Tables 3 and 4]

A charge-transfer will affect the bond lengths and angles of both, the donor and acceptor molecules. Indeed, the data of Tables 3 and 4 confirm the formulation of the complex as $[Vn_2S_2]^+[DDQ]^-$ since they agree well with those of the corresponding radical ions and differ significantly from those of the neutral molecules. This is shown for the donor by the CS and CO distances and the angles in the central dithiin ring, for the acceptor by the CO distance and the beginning equilization of the distances within the six-membered ring.

Crystal structure

From the unit cell of Vn_2S_2·DDQ in Fig. 2 it can be seen that a columnar structure with segregated stacks of the donor and acceptor radical ions is formed in the crystal. The constituents of each stack are coplanarly and equidistantly arranged, their molecular planes being inclined to the stacking axes (Fig. 3). The inclination differs in the donor and acceptor columns, thus leading to different interplanar distances, namely 359 and 308 pm for the donor and acceptor stacks, respectively, both distances being shorter than the van der Waals distance (half thickness of an aromatic nucleus, 185 pm[15]).

[Figures 2 and 3]

In the crystals of $[Vn_2S_2][SbCl_6]\cdot CH_3CN$[10] the radical cations $[Vn_2S_2]^+$, which are also planar, form a different kind of stacks. There are two orientations of the coplanar ions in an alternating sequence AB, AB,..... (angles between the molecular axes, 35°). The interplanar distance (353 pm) agrees well with that in Vn_2S_2·DDQ.

Molecular Orbital (MO) Calculations

In order to arrive at a better understanding of the CT interactions in Vn_2S_2·DDQ, MO calculations were carried out. As already has been shown[16] good results can be obtained by HAM3[17, 18] calculations, whereas the MNDO[19, 20] method normally gives less reliable values for unoccupied orbitals[21-23], *i.e.* too high energy differences between the HOMOs of the donor and the LUMOs of the acceptor molecules are found by MNDO calculations. Nevertheless, with respect to the orbital symmetries, the same energy orders are obtained by both methods, although the absolute values of the orbital energies differ. Since HAM3 parameters have not yet been determinated for elements beyond the second row of the periodic table we decided in favour of MNDO calculations. Furthermore, 2,3,7,8-tetrahydroxythianthrene was taken as a model compound of Vn_2S_2. This seemed tenable, because the expenditure of calculations for the tetramethoxy derivative would be out of all proportion to the attainable improvement on the results.

The frontier orbitals in question, *i.e.* the HOMO of Vn_2S_2 and the LUMO of DDQ, are π-type orbitals and therefore well suitable for CT interactions between parallel planar molecules. These MOs are half-occupied in the radical ions $[Vn_2S_2]^+$ and $[DDQ]^-$. In each

column only orbitals of the same type interact and an optimum overlap would be guaranteed when the molecular planes are perpendicular to the stacking axes. However, probably to achive a closer packing, the molecular planes are inclined to the axes, but apparently in such a way that also in these arrangements the MOs overlap quite well (Fig. 4).

Dielectric Relaxation of the CT Complex

Experimental

Dielectric relaxation measurements by the conventional ac technique were carried out with a Genrad 1689M bridge at 20 frequencies between 10^{-2} and 10^{2} kHz in the temperature range 167-360 K for Vn_2S_2·DDQ and 220-420 K for Vn_2Se_2·DDQ, with steps of 5°C. The sample was moulded into a disc-shaped pill, 1 cm in diameter and 1 mm of thinckness.

Dielectric ac measurements of permittivity ε' and loss factor ε'' show clearly two processes, a low temperatures a dielectric process and at high temperatures a conductive one.

In Fig. 5 ε', ε'' *vs.* T are represented for some frequencies in the range of the dielectric low temperature process for both compounds. From an Arrhenius plot ln f (at the maximum ε'') against T^{-1} (Fig. 6) we obtain 0.22 eV and 0.19 eV for E_a, the energies of activation of Vn_2S_2·DDQ and Vn_2Se_2·DDQ, respectively. In order to obtain more detailed information about this relaxation we have applied the Eyring equation

$$f = \frac{k\,T}{2\pi h}\,\exp\left(\frac{\Delta G}{RT}\right) \qquad (1)$$

where k, h and R are the Boltzmann, Planck and gas constants, respectively, and ΔG is the Gibbs free energy of the barrier to the relaxation process, which is related to the activation enthalpy ΔH and activation entropy ΔS by $\Delta G = \Delta H - T\Delta S$. This leads to

$$ln\frac{f}{T} = ln\frac{k}{2\pi h} + \frac{\Delta S}{R} - \frac{\Delta H}{RT} \qquad (2)$$

where the ΔH and the activation energy E_a given by the Arrhenius equation are related by $E_a = \Delta H + RT$. The values of ΔH and ΔS were directly determined from ln (f/T) *vs.* $1/T$ plots (Fig. 6) and the results obtained are summarizaded in Table 5. Starkweather[24] has held simple relaxations responsible for the processes of low activation entropy.

[Table 5]

The dielectric relaxation process is customarily represented in terms of ε'' against ε' (Cole-Cole plots). Whereas for Debye-type peaks the curves are semicircles, the complex diagram plots representing the dielectric results associated with the dipolar relaxation are skewed arcs, which in many cases approach the real axis through a straight line, described by Havriliak-Negami (HN) equation[25]

$$\varepsilon^* = \varepsilon_\infty + \frac{\varepsilon_0 - \varepsilon_\infty}{\left[1+(i\omega\tau_0)^\alpha\right]^\gamma} \qquad (3)$$

where ε_0 and ε_∞, respectively, represent the relaxated and unrelaxated dielectric permittivity of the relaxation process, τ_0 the relaxation time and α, γ parameters related to the shape and skewness of complex dielectric plot (α is a parameter characterizing a symmetrical broadening of the distribution of relaxation times and γ characterizes an asymmetrical one).

A non linear squares regression (NLSR)[26] was used to improve the data fit. The equivalent electric circuit (in series configuration involving a condenser, C, and a Havriliak-Negami type impedance, $Z_{HN} = [1+(i\omega\tau_0)^\alpha]^\gamma / i\omega[C_0-C_\infty]$) shown in Fig. 7 was employed in order to fit the experimental data and the best set of parameters obtained for both compounds at differents temperatures is given in Table 6. The quality of the fit is demostrated in Fig. 8.

[Figures 7 and 8, Table 6]

The application of the Havriliak-Negami equation to the dielectric loss data $\varepsilon''(\omega)$ provides an adequate functional form to calculate the dipolar correlation function, $\phi(\tau)$. This is due to the fact that the dielectric permittivity is related to the dipole moment time correlation function $\phi(\tau)$ by a one-sided Fourier or pure imaginary Laplace transformation

$$\frac{\varepsilon^*(\omega) - \varepsilon_\infty}{\varepsilon_0 - \varepsilon_\infty} = \int_0^\infty \left[-\frac{d\phi(\tau)}{dt}\right] exp[-i\omega t]dt \qquad (4)$$

where ω ($=2\pi f$) is the angular frequency and the total dipole moment time correlation function $\phi(\tau)$ is given by[27]

$$\phi(\tau) = \frac{\langle \sum \mu_k(0) \cdot \sum \mu_k(t) \rangle}{\left\langle \sum \left(\mu_k(0)\right)^2 \right\rangle} \tag{5}$$

where μ_k is the dipolar moment of each entity (dipole or dipole groups) being assumed to be the same for all the entities.

The time correlation function $\phi(\tau)$ is obtained by a half-sided cosine Fourier transformation

$$\phi(\tau) = \frac{2}{\pi} \int_0^\infty \frac{\varepsilon''(\omega)}{\Delta\varepsilon} \frac{\cos\ \omega t}{\omega}\, d\omega \tag{6}$$

where $\Delta\varepsilon = \varepsilon_0 - \varepsilon_\infty$ is the relaxation strenght.

The numerical evaluation of the preceding equation can be performed by depicting the dipolar process by HN equation for which

$$\begin{aligned} \varepsilon''(\omega) &= \Delta\varepsilon\ r^{-\gamma} \sin \gamma \Psi \\ r^2 &= 1 + 2(\omega\tau)^\alpha \cos\left(\alpha\frac{\pi}{2}\right) + (\omega\tau)^{2\alpha} \\ \tan \Psi &= \frac{(\omega\tau)^\alpha \sin\left(\alpha\frac{\pi}{2}\right)}{1 + (\omega\tau)^\alpha \cos\left(\alpha\frac{\pi}{2}\right)} \end{aligned} \tag{7}$$

where α, γ, τ_0 are parameters obtained with the fit of ε^* to the HN equation.

In order to carry out the fit we have chosen the Kohlrausch-Williams-Watts (KWW)[28,29] function given by

$$\phi(\tau) = exp\left[-\left(\frac{t}{\tau_{KWW}}\right)^\beta\right] \tag{8}$$

where τ_{KWW}, a characteristic relaxation time and β ($0 < \beta \leq 1$), a parameter that describes the non-exponential character of the correlation function, are summarizared in Table 6. It is important to notice that, whereas the β parameters obtained from the KWW function remain practically constant over the entire temperature range, the distribution parameters, α and γ, of

HN equation vary significantly with temperature. This is a consequence of the fact, that different pairs of the α and γ values correspond to each β value because KWW is a single parameter function whereas HN is a two parameters one. The parameters of both functions are related by the following equation

$$(\alpha\gamma)^c = \beta \tag{9}$$

with c = 0.95 and 1.28 for Vn_2S_2.DDQ and Vn_2Se_2.DDQ, respectively.

Curves describing the evolution of this function with time at several temperatures are shown in Fig. 9 .

[Fig.9]

In the high temperature process ε'' continously increases when the frequency diminishes and no relaxation peak is seen. For this reason, the data were modelized using the electrical modulus formalism according to $M^* = (\varepsilon^*)^{-1}$, where

$$M' = \frac{\varepsilon'}{(\varepsilon')^2 + (\varepsilon'')^2}$$
$$M'' = \frac{\varepsilon''}{(\varepsilon')^2 + (\varepsilon'')^2} \tag{10}$$

In the complex electric plot of *M"vs. M'* a nearly exact semi-circle was obtained as can be see from Fig. 10. This proves that the process at high temperature is purely conductive. Accordingly, and following impedance spectroscopy techniques, we tried to fit the experimental data to the electrical model circuit given in Fig. 11 and Table 7.

[Fig.10 and 11, Table 7]

Electrical Conductivity of the CT Complexes

Experimental

The electrical conductivity of both compounds, Vn_2S_2·DDQ and Vn_2Se_2·DDQ, were measured with an HP-4329-A electrometer together with a Guildline 6500 Teraohmmeter by using

silver-coated electrodes on samples moulded at *ca.* 10^8 Pa. The temperature range was 140-370 K; each temperature at which measurements were taken was kept constant by use of a Pt-100 resistence thermometer and an Eurotherm 820 controller.

Results

The results of the conductivity measurements are given in Fig. 12. The absolute values of the conductivities are relatively low, but in both cases the temperature dependence of the conductivity can be described by

$$\sigma = \sigma_0 \cdot \exp(-E_a / 2kT) \qquad (11)$$

where k = Boltzmann's constant, E_a = gap energy, *i.e.* activation energy of the electrical conductivity, and σ_0 = pre-exponential factor, *i.e.* conductivity at infinite temperature. This equation describes a behaviour typical for semiconductors.

The activation energy E_a, obtained from the slope of the Arrhenius plot ($\ln \sigma$ *vs.* $1/T$) of the two conductivities (ac, dc) for both compounds are given in Table 8. We can observe in Fig. 12 that the representation for dc conductivit displays two regions (aproximately at 285 K the slope for both compounds changes significally). A low temperature region where the two activation energies are close ($Ea^{(ac)}$= 0.50 eV, $Ea^{(dc)}$= 0.58 eV for Vn_2S_2.DDQ, $Ea^{(ac)}$= 0.31 eV, $Ea^{(dc)}$= 0.32 eV for Vn_2Se_2.DDQ) and a high temperature region where activation energy rises to approximately 0.83 eV and 0.73 eV for Vn_2S_2.DDQ and Vn_2Se_2.DDQ, respectively. We think that the first region can be explained in terms of an easy-path model and the second region is reached when the conduction through the grain boundaries (having a higher activation energy) exceeds the intragranular conduction. This result (two regions in Arrhenius plot) has also been observed by other authors for polycrystalline materials[26, 30].

The activation energy (intrinsic conductivity) obtained for both compounds are of the same magnitude as the values of similar compounds such as Vn_2S_2·TCNE (0.78 eV) and $2Vn_2S_2$·TCNE (0.95 eV). Due to the fact that the charge of the donor and aceptor molecules is stoichometric (+1 and -1, respectively), the conductivities of the compounds Vn_2E_2·DDQ (E = S, Se) are not very high, though significantly higher than in other compounds thus as Vn_2E_2·TCNQ and $2Vn_2E_2$·TCNE (Table 8).

The central problem with ac measurements arises from the interpretation of the data. This is because the sample and electrode arrangement is electrically a "black box" the equivalent circuit of which (*i.e.* its representation by some combination of R and C elements) is often unknow. The crux of the problem in analyzing ac data is (a) to determine the appropiate equivalent circuit for the cell and (b) evaluate the various R and C components in the electric circuit. In polycrystalline materials the overall sample resistence may be a combination of the intragranular resistence (or bulk crystal resistence) and the intergranular (or grain boundary) resistence. Both resistences are parallel with an associated capacitance, and each parallel RC element gives rise to a semi-circle in the complex plane Z*. In the frequency range in which we worked , we can observe only one semi-circle associated at grain interior conductivity (intrinsic conductivity), for this reason we employed the simple parallel RC element (Fig. 11).

This work has been supported by the Acción Integrada Hispano-Alemana (N° HA94-103, 322-ai-e-dv). We also thank the Volkswagenstiftung and the Fonds der Chemischen Industrie for financial suppors. M. Dötze greatfully acknowledges the grant by DAAD (NATO-fonds). Maria J. Sanchis acknowledges the Consellería de Educación y Ciencia de la Generalitat Valenciana for a grant.

References

1 Part 6: J. Behrens, W. Hinrichs, T. Link, C. Schiffling and G. Klar, *Phosphorus, Sulfur and Silicon*, 1995, **101**, 235.

2 P. Berges, J. Kudnig, G. Klar, E. Sánchez Martínez and R. Díaz Calleja, *Z. Naturforsch., Teil B,* 1989, **44**, 211.

3 W. Hinrichs and G. Klar, *J. Chem. Res.*, 1982, (*S*) 336, (*M*) 3540.

4 W. Hinrichs, P. Berges, G. Klar, E. Sánchez Martínez and W. Gunβer, *Synth. Met.* 1987, **20**, 357.

5 E. Sánchez Martínes, R. Díaz Calleja, W. Gunβer, P. Berges and G. Klar, *Synth. Met.* 1989, **30**, 67.

6 W. Gunβer, J.H. Henning, G. Klar and E. Sánchez Martínez, *Ber. Bunsenges. Phys. Chem.*, 1989, **93**, 1370.

7 G.M. Sheldrik, SHELXTL-Plus, Release 4.21/0, Copyright 1990 Siemens Analytical X-Ray Instruments.

8 W. Hinrichs, H.-J. Riedel and G. Klar, *J. Chem. Res.*, 1982, *(S)* 334, *(M)* 3501.

9 H. Bock, A. Rauschenbach, C. Näther, Z. Havlas, A.Gavezzotti and G. Filippini, *Angew. Chem.*, 1995, **107**, 120, *Int. Ed. Engl.* **34**, 76.

10 W. Hinrichs, P. Berges and G. Klar, *Z. Naturforsch., Teil B*, 1987, **42**, 169.

11 M.E. Peover, *J. Chem. Soc.*, 1962, 4540.

12 R.C. Wheland and J.L. Gillson, *J. Am. Chem. Soc.*, 1976, **98**, 3916.

13 G. Zanotti, A. Del Pra and R. Bozio, *Acta Crystallogr., Sect B.*, 1982, **38**, 1225.

14 G. Zanotti, R. Bardi and A. Del Pra, *Acta Crystallogr. Sect.B*, 1980, **36**, 168.

15 *Handbook of Chemistry and Physics*, CRC Press Cleveland, OH, 58th edn., 1977-1978, p. D-178.

16 E. Sánchez Martínez, R. Díaz Calleja, P. Berges, J. Kudning and G. Klar, *Synth. Met.*, 1989, **32**, 79.

17 L. Åsbrink, C. Fridh and E. Lindholm, *Chem. Phys. Lett.*, 1977, **52**, 63; **69**, 72.

18 L. Åsbrink, C. Fridh and E. Lindholm, *QCPE Bull.*, 1980, **12**, 393.

19 M.J.S.Dewar and W.Thiel, *J.Am.Chem.Soc.*, 1977, **99**, 4899; 4907.

20 W.Thiel, *QCPE Bull.*, 1982, **2**, 438.

21 L. Åsbrink, C. Fridh and E. Lindholm, *Chem. Phys.*, 1978, **27**, 169.

22 C.Fridh, L. Åsbrink and E. Lindholm, *Chem. Phys.*, 1978, **27**, 159.

23 E. Lindholm, G. Bieri, L. Åsbrink and C. Fridh, *Int. J. Quant. Chem.*, 1978, **14**, 737.

24 H. W. Starkweather, Jr., *Macromolecules*, 1981, **14**, 1277;1990, **23**, 328.

25 S. Havriliak and S. Negami, *Polymer*, 1967, **8**, 161.

26 J. Ross McDonald, *Complex Nonlinear Least Squares Immitance Fitting Program, LEVM6*, 1993; *Impedance Spectroscopy*, Wiley-Interscience, New York, 1987.

27 G.Williams, *Chem. Soc. Rev.*, 1978, **7**, 89.

28 G. Williams and D. C. Watts, *Trans. Faraday Soc.*, 1970, **66**, 80.

29 R. Kohlrausch, *Pogg. Ann. Phys. Chem.*, 1884, **91**, 179.

30 A. R. West, *Solid State Chemistry and its Applications*, Wiley, 1984, chapter 13.

31 E. Sánchez Martínez, R. Díaz Calleja and G. Klar, *Synth. Met.*, 1990, **38**, 93.

32 E. Sánchez Martínez, R. Díaz Calleja, J. Behrens, P. Berges, J. Kdnig, N. Wölki and G. Klar, *J. Chem. Res.*, 1991, (*S*) 246, (*M*) 2379.

Figure Captions

Figure 1. Molecular structures of the components of Vn_2S_2·DDQ with scheme of atom numbering

Figure 2. Contents of the unit cell of Vn_2S_2·DDQ

Figure 3. Segregated stacks of donors and acceptors in Vn_2S_2·DDQ. (a) top view; (b) side view

Figure 4. (a) Relative positions of two successive donors and acceptors, resp., in the stacks of Vn_2S_2·DDQ; (b) overlap of the corresponding frontier orbitals

Figure 5. Temperature dependence of the dielectric permittivity ε' and loss ε'' (a) of Vn_2S_2·DDQ and (b) Vn_2Se_2·DDQ at various frequencies (● 100 Hz, × 50 Hz, ■ 20 Hz, + 10 Hz, ♦ 5 Hz

Figure 6. Temperature dependence of $f_{\varepsilon''}$. (a) According to Arrhenius's equation; (b) according to Eyring's equation for Vn_2S_2·DDQ (o, ●) and Vn_2Se_2·DDQ (□,■)

Figure 7. Electrical circuit representing the dielectric process at low temperatures

Figure 8. Cole-Cole plot at 220 K for Vn_2S_2·DDQ (o experimental data, • calculated data)

Figure 9. Normalized correlation function calculated according to HN equation and KWW equation for Vn_2S_2·DDQ (o, ●) and Vn_2Se_2·DDQ (□,■)

Figure 10. *M' vs. M"*(Cole-Cole) plot at 360 K for Vn_2S_2·DDQ (o experimental data, ● calculated data)

Figure 11. Electrical circuit to represent the conductive process at high tempertures

Figure 12. Arrhenius plot of $\ln \sigma^{ac}$, $\ln \sigma^{dc}$ vs 1/T for Vn_2S_2·DDQ (o, ●) and Vn_2Se_2·DDQ (□,■)

2,3,7,8–Tetramethoxythianthrene – 2,3–Dichloro-5,6-dicyano-1,4-benzoquinone 1:1 Charge-transfer Complex

Supplementary data

To be deposited with the Cambridge Crystallographic Data Centre.

Notice

We apologize for not being in a position to send the data by E-mail because the structure determination has been done some years ago.

Table 1. Crystal Structure parameters of Vn_2S_2·DDQ

empirical formula	$C_{16}H_{16}O_4S_2 \cdot C_8Cl_2N_2O_2$
crystal system	monoclinic
space group	P_2/c
a / pm	370.8(2)
b / pm	1306.9(6)
c / pm	2355.7(11)
β / degrees	93.50(4)
Z	2
M / g mol^{-1}	563.4
V / m^3	$1139 \cdot 10^6$
D / g cm^{-3}	1.642
μ / cm^{-1}	5.16
scan range/ degrees	$5 < 2\theta < 50$
independent reflections	2037
reflections with $\|F_0\| \geq 4\sigma(\|F_0\|)$	1548
refined parameters	165
R	0.0473
R_w	0.0436

Table 2. Atomic parameters of Vn_2S_2·DDQ

atom	*x/a*	*y/b*	*z/c*
S(1)	0.3579(4)	0.5294(1)	0.4307(1)
C(11)	0.4485(11)	0.4088(2)	0.4581(1)
C(12)	0.5774(11)	0.3853(2)	0.5138(1)
C(13)	0.6589(10)	0.2839(3)	0.5287(1)
C(14)	0.6126(9)	0.2072(3)	0.4892(1)
C(15)	0.4765(10)	0.2307(2)	0.4327(1)
C(16)	0.3924(10)	0.3298(2)	0.4181(1)
O(14)	0.6890(7)	0.1078(2)	0.4991(1)
C(17)	0.8389(11)	0.0823(3)	0.5550(1)
O(15)	0.4368(7)	0.1496(2)	0.3968(1)
C(18)	0.2780(11)	0.1699(3)	0.3410(1)
Cl(32)	0.2668(3)	0.9085(1)	0.1914(1)
C(31)	0.2658(10)	0.7019(3)	0.1969(1)
C(32)	0.3949(9)	0.7968(2)	0.2251(1)
C(36)	0.3878(10)	0.6091(2)	0.2254(2)
O(31)	0.0632(7)	0.7022(2)	0.1533(1)
C(38)	0.2696(10)	0.5141(3)	0.2005(1)
N(38)	0.1723(9)	0.4370(2)	0.1821(1)

Table 3. Mean values of bond lengths (pm) and angles (degrees) in the donor molecule of Vn_2S_2·DDQ and comparative compounds

	Vn_2S_2· DDQ	$[Vn_2S_2]^+[SbCl_6]^-$ [a]	Vn_2S_2 [b]
S-C	172.6(3)	172.3(5)	177.6(7)
O-C (ar)	135.2(4)	134.9(5)	136.9(8)
O-C (alk)	143.4(4)	143.3(5)	142.5(9)
C(S)-C(S)	140.3(5)	139.5(6)	138.2(10)
C(S)-C(H)	140.3(5)	140.0(6)	139.7(9)
C(H)-C(O)	137.1(4)	136.2(6)	138.0(10)
C(O)-C(O)	142.8(5)	143.0(7)	141.0(10)
C-S-C	107.0(2)	107.4(3)	100.2(3)
C-O-C	116.8(3)	118.0(4)	117.6(5)
S-C(S)-C(S)	126.3(3)	126.0(4)	121.1(5)
S-C(S)-C(H)	113.9(2)	114.9(4)	119.0(5)
O-C(O)-C(O)	115.5(3)	114.5(5)	115.2(6)
O-C(O)-C(H)	124.7(3)	125.9(5)	125.2(6)
C(S)-C(S)-C(O)	119.7(3)	119.5(4)	119.8(6)
C(S)-C(H)-C(O)	120.4(3)	120.0(5)	120.5(6)
C(H)-C(O)-C(O)	119.9(3)	119.6(5)	119.6(6)

[a] Ref. 10 . [b] Ref. 8.

Table 4. Mean values of bond lengths (pm) and angles (degrees) in the acceptor molecule of Vn_2S_2· DDQ and comparative compounds

	Vn_2S_2· DDQ	$[Vn_2S_2]^+[SbCl_6]^-$ [a]	Vn_2S_2 [b]
C-Cl	171.5(3)	171.6(3)	169.7(3)
C-O	123.6(4)	124.6(4)	120.3(3)
C-N	114.7(5)	114.0(4)	113.4(4)
C-C(N)	143.0(5)	143.0(5)	143.6(4)
C(Cl)-C(Cl)	136.8(6)	136.3(4)	133.9(4)
C(CN)-C(CN)	138.6(7)	138.6(4)	134.3(4)
C(Cl)-C(O)	147.2(5)	146.3(4)	148.2(4)
C(CN)-C(O)	144.5(5)	144.4(4)	149.7(4)
N-C-C	178.0(4)	178.4(4)	178.5(3)
Cl-C-C(Cl)	121.6(1)	121.8(2)	122.8(2)
Cl-C-C(O)	115.8(2)	115.7(2)	115.5(2)
O-C-C(Cl)	122.5(3)	122.6(3)	123.3(2)
O-C-C(CN)	123.0(3)	122.6(3)	119.8(2)
C(N)-C-C(CN)	119.7(2)	120.7(3)	122.8(2)
C(N)-C-C(O)	117.4(3)	116.8(3)	115.9(2)
C(Cl)-C(Cl)-C(O)	122.6(2)	122.6(3)	121.7(2)
C(Cl)-C(O)-C(CN)	114.5(3)	114.9(3)	117.0(2)
C(Cl)-C(CN)-C(CN)	122.9(2)	122.6(3)	121.3(2)

[a] Ref. 13 . [b] Ref. 14.

Table 5. Eyring's Equation Parameters

Compound	ΔH / eV	E_a / eV	ΔS / meV K^{-1}
Vn_2S_2·DDQ	0.2037	0.2212	0.0028
Vn_2Se_2·DDQ	0.1772	0.1946	0.0027

Table 6. Havriliak-Negami Parameters equation $\Delta\varepsilon$, α, γ, τ_{HN} and Kohlrausch-Williams-Watts Parameters β, τ_{KWW} for the CT complexes

Vn_2S_2·DDQ

T / K	ε_∞	ε_0	$\Delta\varepsilon$	α	γ	τ_{HN} / s	β	τ_{KWW} / s
190	3.08	118.83	121.91	0.79	0.72	$2.15\ 10^{-4}$	0.584	$1.45\ 10^{-4}$
200	2.65	117.32	119.97	0.79	0.69	$1.17\ 10^{-4}$	0.569	$7.38\ 10^{-5}$
210	2.67	118.31	120.98	0.76	0.71	$7.02\ 10^{-5}$	0.557	$4.78\ 10^{-5}$
220	2.79	121.48	124.27	0.78	0.70	$4.75\ 10^{-5}$	0.561	$3.08\ 10^{-5}$

Vn_2Se_2·DDQ

T / K	ε_∞	ε_0	$\Delta\varepsilon$	α	γ	τ_{HN} / s	β	τ_{KWW} / s
220	6.36	75.12	81.49	0.72	0.90	$2.58\ 10^{-5}$	0.570	$2.72\ 10^{-5}$
230	8.29	65.53	73.82	0.77	0.96	$1.38\ 10^{-5}$	0.669	$1.47\ 10^{-5}$
240	9.88	62.48	72.36	0.79	0.87	$6.42\ 10^{-6}$	0.655	$5.89\ 10^{-6}$

Table 7. Parameters for the model of the Fig. 11 giving the best fit with the experimental data for both CT complexes at different temperatures

	Vn_2S_2·DDQ			**Vn_2Se_2·DDQ**		
T / K	R	$C.10^9$	M_∞	R	$C.10^{10}$	M_∞
330	$1.32\ 10^7$	0.1287	0.00777			
340	$8.84\ 10^6$	0.1288	0.00776	$1.98\ 10^7$	0.9132	0.01095
350	$8.55\ 10^6$	0.1314	0.00761	$1.58\ 10^7$	0.8974	0.01114
360	$6.43\ 10^6$	0.1327	0.00754	$1.47\ 10^7$	0.8870	0.01127
370				$1.43\ 10^7$	0.8708	0.01148

Table 8. Conductivity data of some Vn_2E_2 derivatives

Compound	E_a /eV	σ_0/ S cm^{-1}	σ_{293K}/ S cm^{-1}
Vn_2S_2· DDQ	0.58	2.09	$4.88\ 10^{-6}$
Vn_2Se_2· DDQ	0.32	0.012	$8.60\ 10^{-6}$
Vn_2S_2· TCNQ[a]	0.78	0.04	$8.20\ 10^{-9}$
Vn_2Se_2· TCNQ[a]	0.84	0.012	$6.12\ 10^{-10}$
$2Vn_2S_2$· TCNE[b]	1.27	0.95	$1.11\ 10^{-11}$
$2Vn_2Se_2$· TCNE[b]	1.17	0.96	$8.32\ 10^{-12}$
Vn_2Se_2· Br_2[c]	1.07	0.0025	$4.3\ 10^{-5}$
DNDT[d]	0.96	738	$7.0\ 10^{-12}$

[a]Ref. 3. [b]Ref. 2. [c]Ref.31. [d]DNDT = dinaphtho[2,3-b;2′,3′-*e*] [1,4] dithiin-5,7,12,14-tetraone.[32]

illustration for contents

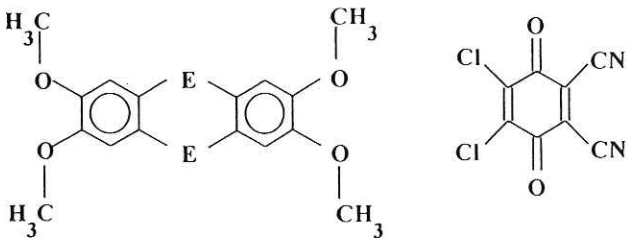

$Vn_2E_2 \cdot DDQ$ (E= S, Se)

formulae

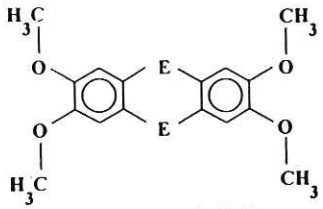

Vn_2E_2 (E = S, Se)

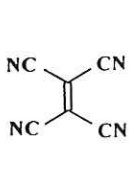

TCNE

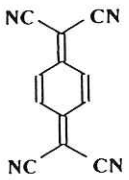

TCNQ

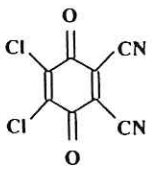

DDQ

Fig. 1

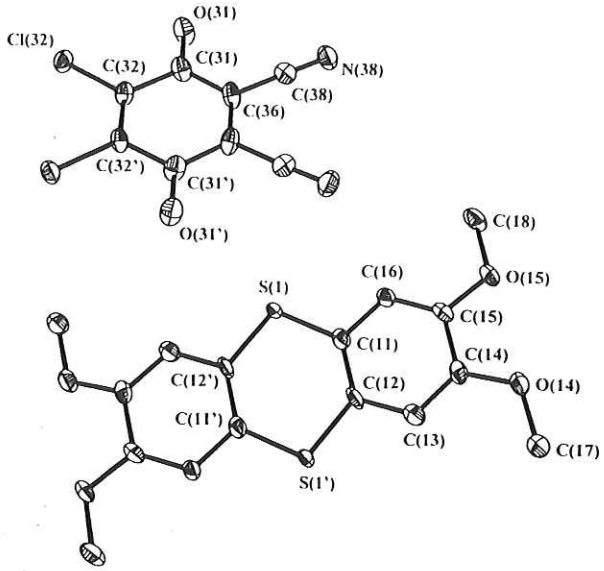
O(31)
Cl(32)
C(32)
C(31)
N(38)
C(38)
C(36)
C(32')
C(31')
O(31')
C(18)
C(16)
O(15)
S(1)
C(15)
C(11)
C(14)
C(12')
C(12)
O(14)
C(11')
C(13)
C(17)
S(1')

Fig. 2

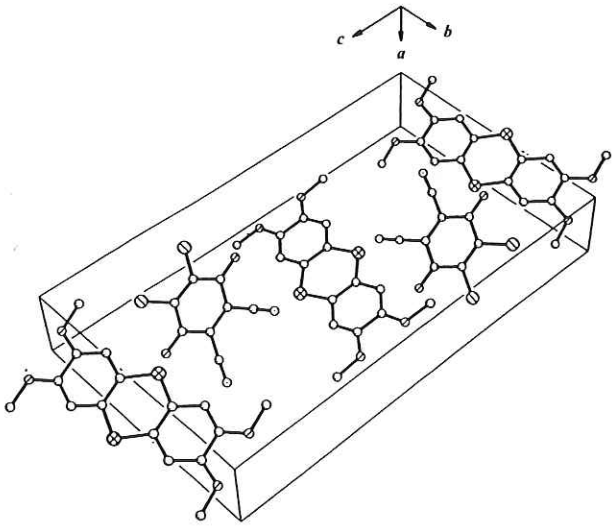
c
b
a

Fig. 3

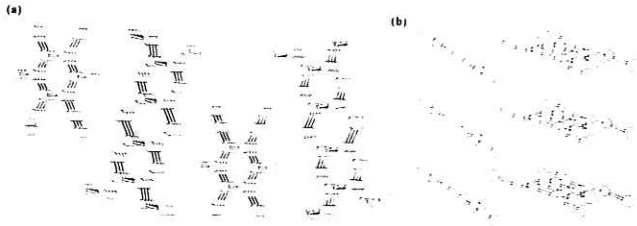

Fig. 4

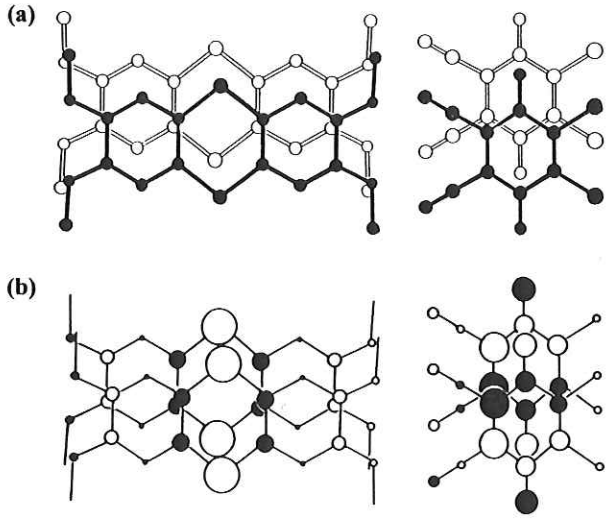

Fig. 5

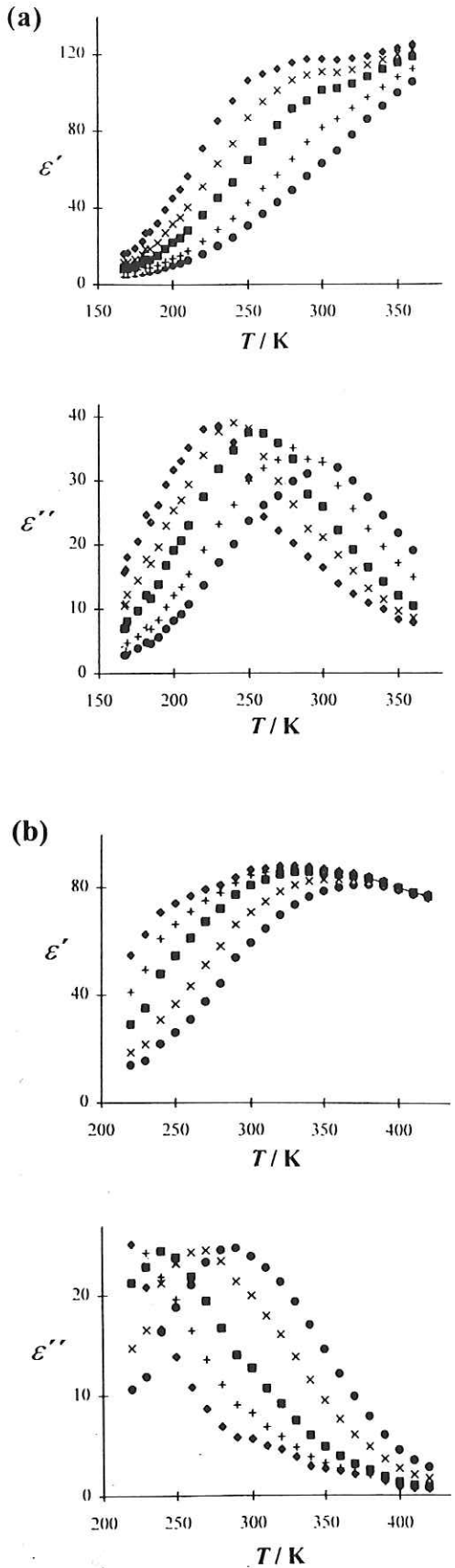
(a)
120
80
40
0
ε′
150
200
250
300
350
T / K
40
30
20
10
0
ε″
150
200
250
300
350
T / K
(b)
80
40
0
ε′
200
250
300
350
400
T / K
20
10
0
ε″
200
250
300
350
400
T / K

Fig. 6

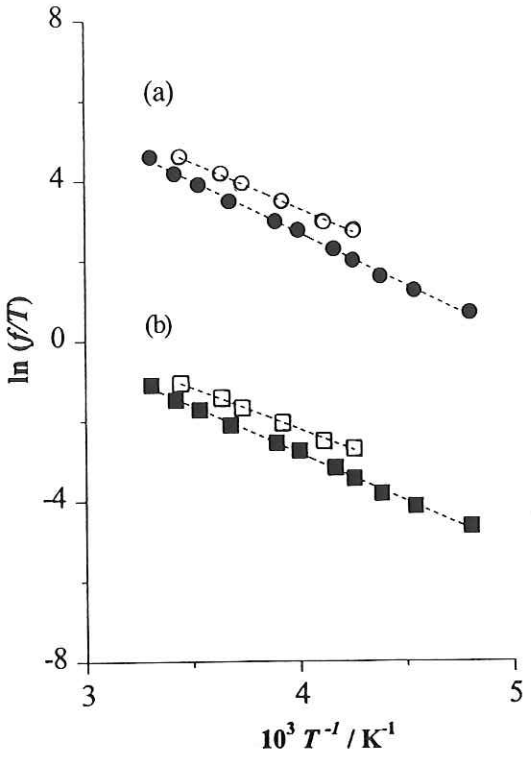

Fig. 7

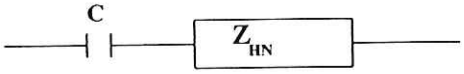

Fig. 8

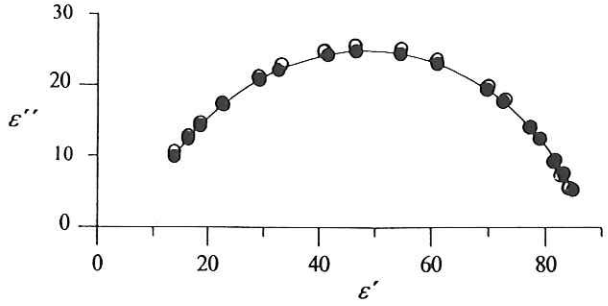

Fig.9

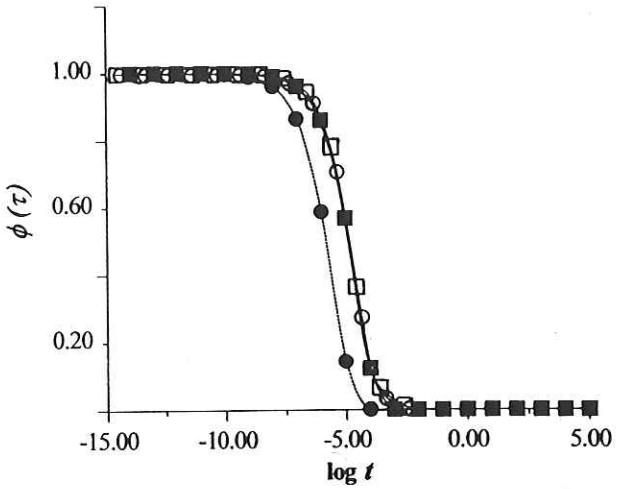

Fig.10

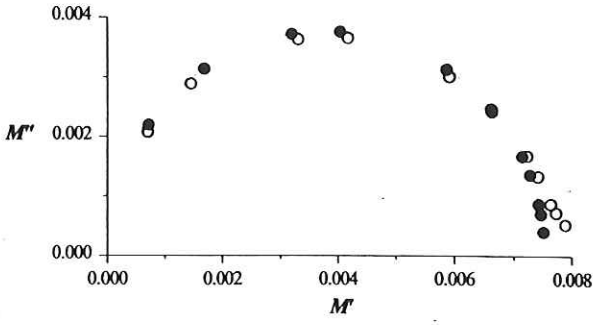

Fig. 11

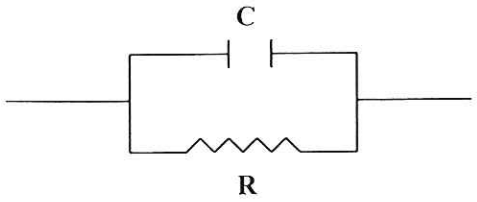
C
R

Fig. 12

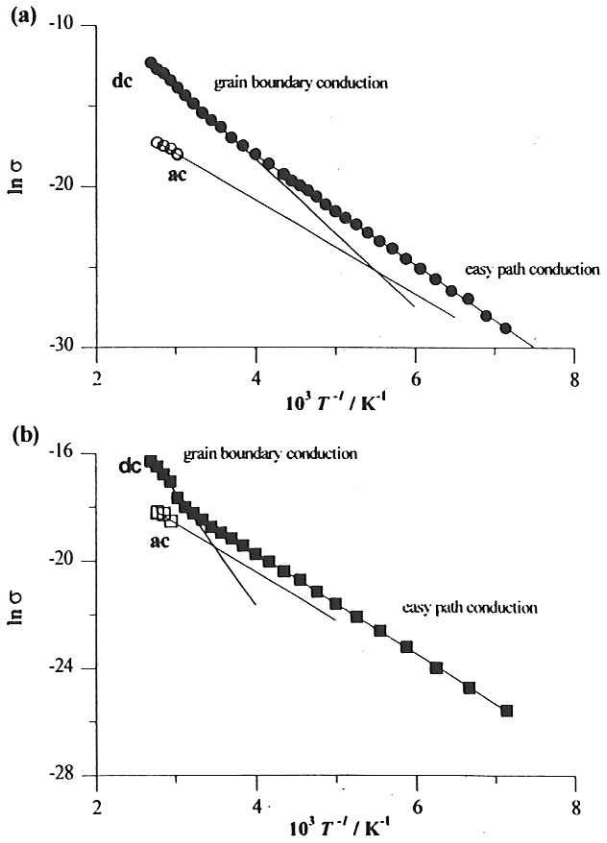
(a)
-10
-20
-30
ln σ
dc
grain boundary conduction
ac
easy path conduction
2
4
6
8
10³ T⁻¹ / K⁻¹
(b)
-16
-20
-24
-28
ln σ
dc
grain boundary conduction
ac
easy path conduction
2
4
6
8
10³ T⁻¹ / K⁻¹

2,3,7,8–Tetramethoxythianthrene – 2,3–Dichloro-5,6-dicyano-1,4-benzoquinone 1:1 Charge-transfer Complex

Supplementary data

To be deposited with the Cambridge Crystallographic Data Centre.

Notice

We apologize for not being in a position to send the data by E-mail because the structure determination has been done some years ago.

STRUCTURE DETERMINATION SUMMARY

Crystal Data

Empirical Formula	$C_{24}\ H_{16}\ Cl_2\ N_2\ O_6\ S_2$
Color; Habit	Black needles
Crystal Size (mm)	0.8 x 0.6 x 0.4
Crystal System	Monoclinic
Space Group	P2/c
Unit Cell Dimensions	$\underline{a}$ = 3.708(2) Å
	$\underline{b}$ = 13.069(6) Å
	$\underline{c}$ = 23.557(11) Å
	β = 93.50(4)°
Volume	1139.3(10) $Å^3$
Z	2
Formula Weight	563.4
Density(calc.)	1.642 Mg/m^3
Absorption Coefficient	0.516 mm^{-1}
F(000)	576

Data Collection

Diffractometer Used	Siemens P4
Radiation	MoKα (λ = 0.71073 Å)
Temperature (K)	153
Monochromator	Highly oriented graphite crystal
2θ Range	5.0 to 50.0^{o}
Scan Type	2θ–θ
Scan Speed	Variable; 4.99 to 29.30^{o}/min. in ω
Scan Range (ω)	1.00^{o} plus Kα-separation
Background Measurement	Stationary crystal and stationary counter at beginning and end of scan, each for 25.0% of total scan time
Standard Reflections	3 measured every 197 reflections
Index Ranges	$-4 \leq h \leq 4$, $-6 \leq k \leq 15$ $-28 \leq \ell \leq 28$
Reflections Collected	4312
Independent Reflections	2037 (R_{int} = 2.54%)
Observed Reflections	1548 ($F > 4.0\sigma(F)$)

Solution and Refinement

System Used	Siemens SHELXTL PLUS (VMS)
Solution	Direct Methods
Refinement Method	Full-Matrix Least-Squares
Quantity Minimized	$\sum w(F_o - F_c)^2$
Hydrogen Atoms	Riding model, fixed isotropic U
Weighting Scheme	$w^{-1} = \sigma^2(F) + 0.0001F^2$
Number of Parameters Refined	165
Final R Indices (obs. data)	R = 4.73 %, wR = 4.36 %
R Indices (all data)	R = 6.78 %, wR = 4.68 %
Goodness-of-Fit	1.66
Largest and Mean Δ/σ	0.011, 0.003
Data-to-Parameter Ratio	9.4:1
Largest Difference Peak	0.53 $e\text{Å}^{-3}$
Largest Difference Hole	-0.70 $e\text{Å}^{-3}$

Table 1. Atomic coordinates ($x10^5$) and equivalent isotropic displacement coefficients (pm^2)

	x	y	z	U(eq)
S(1)	35789(39)	52940(7)	43073(4)	478(4)
C(11)	44854(106)	40884(24)	45808(14)	260(10)
C(12)	57743(111)	38535(23)	51380(14)	270(11)
C(13)	65888(96)	28389(26)	52869(14)	249(11)
C(14)	61260(92)	20717(25)	48916(14)	220(10)
C(15)	47645(95)	23074(24)	43266(14)	209(10)
C(16)	39244(98)	32976(23)	41813(13)	229(10)
O(14)	68895(71)	10782(16)	49912(9)	275(8)
C(17)	83889(107)	8225(28)	55497(13)	300(11)
O(15)	43679(71)	14962(17)	39677(9)	279(8)
C(18)	27802(110)	16985(27)	34099(14)	313(11)
Cl(32)	26680(27)	90849(6)	19137(3)	254(3)
C(31)	26584(100)	70192(26)	19693(15)	266(11)
C(32)	39494(88)	79679(24)	22510(13)	206(10)
C(36)	38779(95)	60909(24)	22537(15)	250(10)
O(31)	6319(74)	70215(18)	15330(11)	338(8)
C(38)	26960(98)	51410(26)	20053(14)	234(10)
N(38)	17225(92)	43698(23)	18214(13)	331(11)

* Equivalent isotropic U defined as one third of the trace of the orthogonalized U_{ij} tensor

Table 2. Bond lengths (pm)

S(1)-C(11)	172.8	(3)	S(1)-C(12A)	172.3	(3)
C(11)-C(12)	140.3	(5)	C(11)-C(16)	140.5	(5)
C(12)-C(13)	140.0	(5)	C(12)-S(1A)	172.3	(3)
C(13)-H(13)	105.0		C(13)-C(14)	137.2	(5)
C(14)-C(15)	142.8	(5)	C(14)-O(14)	134.6	(4)
C(15)-C(16)	137.0	(4)	C(15)-O(15)	135.8	(4)
C(16)-H(16)	105.0		O(14)-C(17)	143.6	(4)
C(17)-H(171)	105.0		C(17)-H(172)	105.0	
C(17)-H(173)	105.0		O(15)-C(18)	143.1	(4)
C(18)-H(181)	105.0		C(18)-H(182)	105.0	
C(18)-H(183)	105.0		Cl(32)-C(32)	171.5	(3)
C(31)-C(32)	147.2	(5)	C(31)-C(36)	144.5	(5)
C(31)-O(31)	123.6	(4)	C(32)-C(32A)	136.8	(6)
C(36)-C(38)	143.0	(5)	C(36)-C(36A)	138.6	(7)
C(38)-N(38)	114.7	(5)			

Table 3. Bond angles (°)

C(11)-S(1)-C(12A)	107.0(2)	S(1)-C(11)-C(12)	126.6(3)
S(1)-C(11)-C(16)	113.8(2)	C(12)-C(11)-C(16)	119.6(3)
C(11)-C(12)-C(13)	119.8(3)	C(11)-C(12)-S(1A)	126.3(2)
C(13)-C(12)-S(1A)	113.9(3)	C(12)-C(13)-H(13)	119.8(2)
C(12)-C(13)-C(14)	120.4(3)	H(13)-C(13)-C(14)	119.8(2)
C(13)-C(14)-C(15)	119.8(3)	C(13)-C(14)-O(14)	124.8(3)
C(15)-C(14)-O(14)	115.4(3)	C(14)-C(15)-C(16)	119.9(3)
C(14)-C(15)-O(15)	115.5(3)	C(16)-C(15)-O(15)	124.6(3)
C(11)-C(16)-C(15)	120.4(3)	C(11)-C(16)-H(16)	119.8(2)
C(15)-C(16)-H(16)	119.8(2)	C(14)-O(14)-C(17)	116.7(3)
O(14)-C(17)-H(171)	109.5(2)	O(14)-C(17)-H(172)	109.5(2)
H(171)-C(17)-H(172)	109.5(1)	O(14)-C(17)-H(173)	109.5(2)
H(171)-C(17)-H(173)	109.5(1)	H(172)-C(17)-H(173)	109.5(1)
C(15)-O(15)-C(18)	116.8(3)	O(15)-C(18)-H(181)	109.5(2)
O(15)-C(18)-H(182)	109.5(2)	H(181)-C(18)-H(182)	109.5(1)
O(15)-C(18)-H(183)	109.5(2)	H(181)-C(18)-H(183)	109.5(1)
H(182)-C(18)-H(183)	109.5(1)	C(32)-C(31)-C(36)	114.5(3)
C(32)-C(31)-O(31)	122.5(3)	C(36)-C(31)-O(31)	123.0(3)
Cl(32)-C(32)-C(31)	115.8(2)	Cl(32)-C(32)-C(32A)	121.6(1)
C(31)-C(32)-C(32A)	122.6(2)	C(31)-C(36)-C(38)	117.4(3)
C(31)-C(36)-C(36A)	122.9(2)	C(38)-C(36)-C(36A)	119.7(2)
C(36)-C(38)-N(38)	178.0(4)		

Table 4. Anisotropic displacement coefficients (pm^2)

	U_{11}	U_{22}	U_{33}	U_{12}	U_{13}	U_{23}
S(1)	1152(11)	148(4)	145(5)	-155(6)	133(6)	-46(4)
C(11)	373(21)	181(16)	240(17)	-100(17)	128(16)	-35(14)
C(12)	420(23)	159(16)	242(17)	-98(18)	111(17)	-106(14)
C(13)	277(20)	251(18)	224(17)	-64(17)	61(16)	-45(15)
C(14)	206(18)	163(15)	295(18)	-47(15)	58(15)	-39(14)
C(15)	208(18)	229(17)	196(16)	-56(16)	54(15)	-86(14)
C(16)	313(20)	179(16)	201(17)	-82(16)	54(16)	-33(13)
O(14)	356(15)	193(12)	269(13)	49(12)	-45(11)	-61(10)
C(17)	387(22)	258(18)	251(18)	43(19)	-21(17)	-37(16)
O(15)	402(16)	193(12)	238(12)	-8(12)	-26(11)	-93(10)
C(18)	353(22)	308(19)	267(19)	26(19)	-73(17)	-127(16)
Cl(32)	295(5)	195(4)	266(4)	28(4)	-22(3)	44(3)
C(31)	222(19)	248(17)	316(20)	-10(18)	-79(17)	-45(16)
C(32)	145(17)	161(15)	306(18)	42(15)	-33(14)	20(14)
C(36)	170(18)	189(16)	382(20)	-13(15)	-44(15)	-47(14)
O(31)	378(15)	259(13)	350(14)	60(13)	-194(12)	-50(12)
C(38)	167(18)	273(18)	263(18)	-34(17)	32(15)	-31(15)
N(38)	402(21)	246(16)	355(18)	-47(15)	94(16)	-72(14)

The anisotropic displacement factor exponent takes the form:

$-2\pi^2(h^2a^{*2}U_{11} + \ldots + 2hka^*b^*U_{12})$

Table 5. H-Atom coordinates ($x10^4$) and isotropic displacement coefficients ($pm^2 x10^{-1}$)

	x	y	z	U
H(13)	7560	2664	5704	32(7)
H(16)	2855	3467	3769	32(7)
H(171)	8863	31	5574	41(5)
H(172)	6566	1033	5853	41(5)
H(173)	10835	1216	5630	41(5)
H(181)	2622	1015	3175	41(5)
H(182)	4380	2229	3204	41(5)
H(183)	174	1999	3441	41(5)

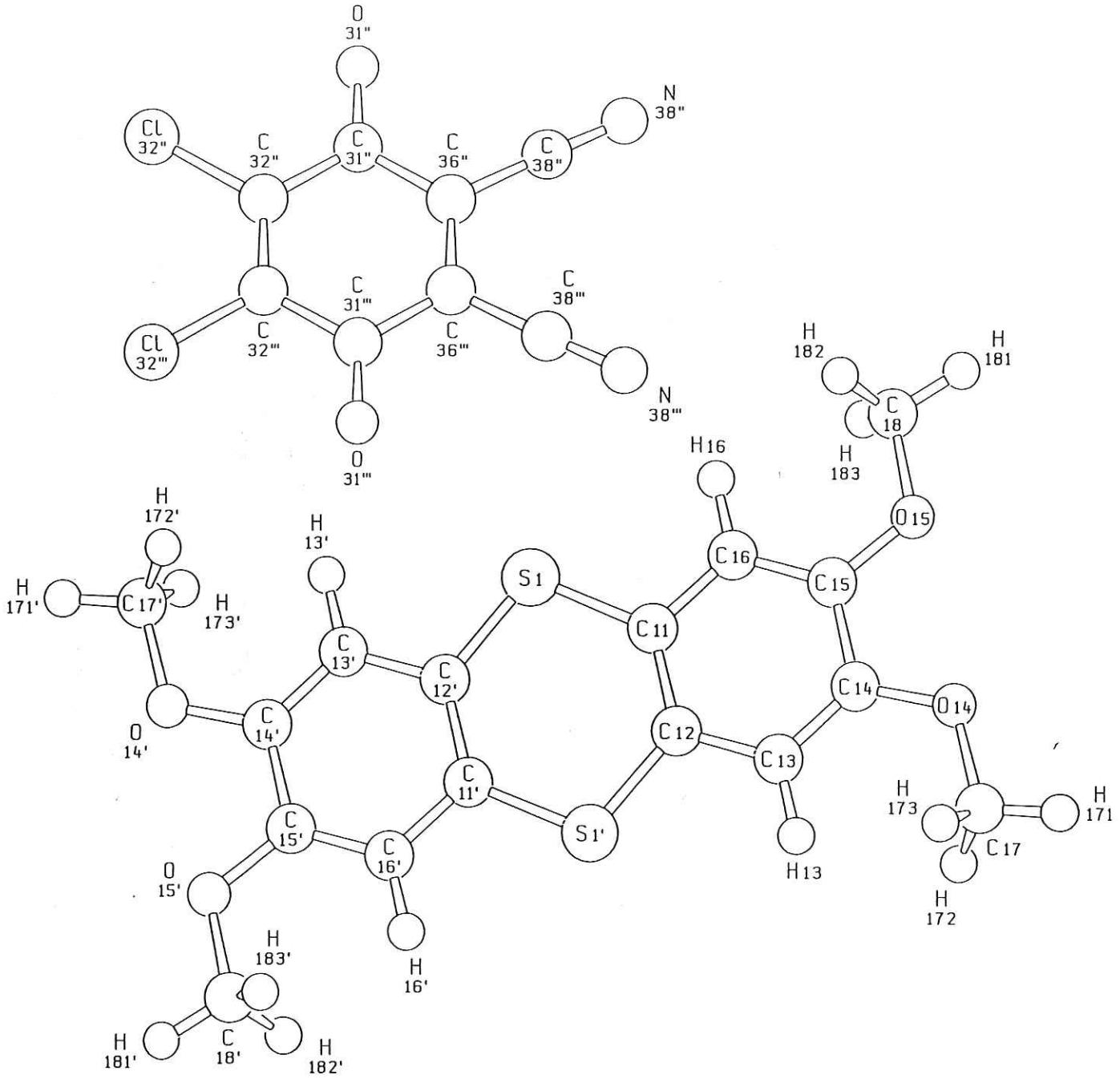
O 31"
N 38"
Cl 32"
C 32"
C 31"
C 36"
C 38"
C 31'''
C 38'''
Cl 32'''
C 32'''
C 36'''
N 38'''
O 31'''
H 182
H 181
C 18
H 183
H16
O15
H 172'
H 13'
H 171'
C17'
H 173'
S1
C16
C15
C11
C 13'
C 12'
C14
O14
O 14'
C 14'
C12
C13
C 11'
H 173
H 171
C 15'
S1'
C17
O 15'
C 16'
H13
H 172
H 183'
H 16'
H 181'
C 18'
H 182'

SCHAKAL

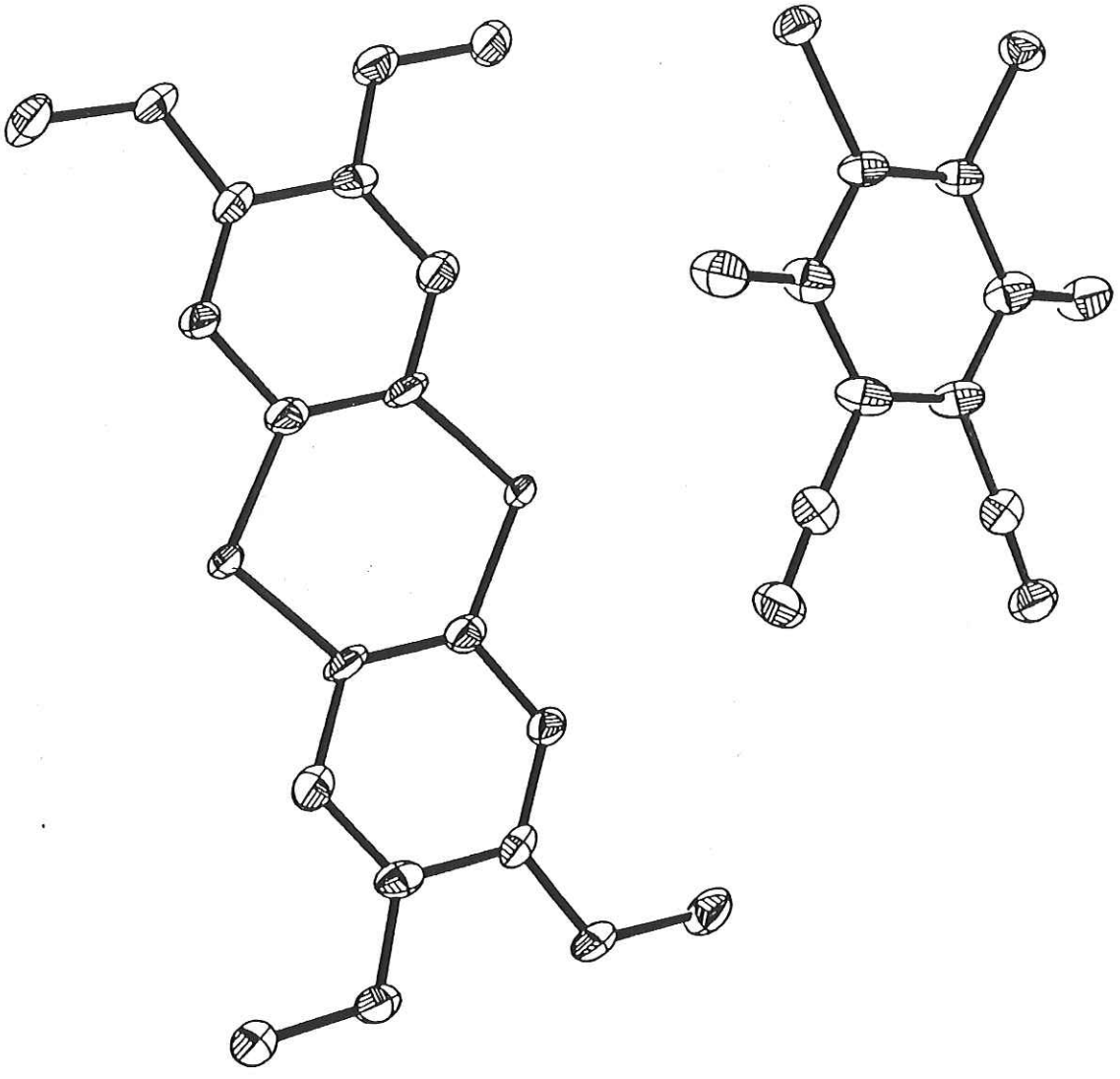

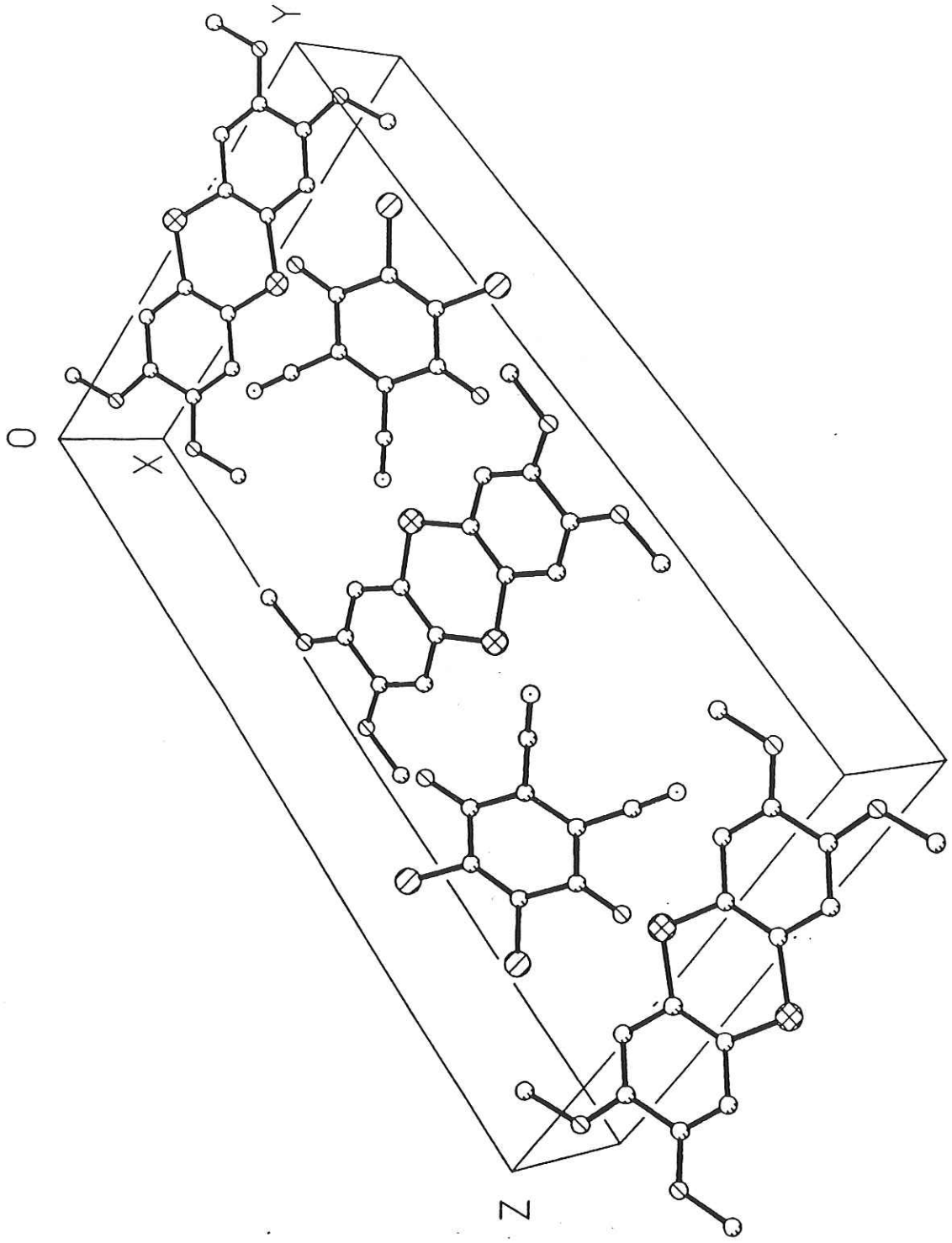
Y
O
X
Z